ChemComm

Accepted Manuscript

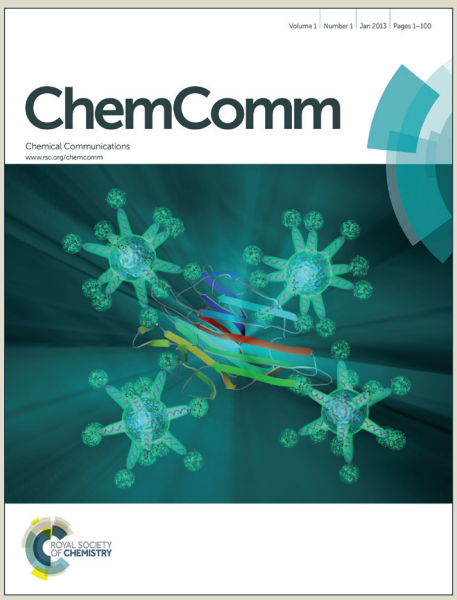

ROYAL SOCIETY OF CHEMISTRY

www.rsc.org/chemcomm

Journal Name

RSCPublishing

COMMUNICATION

Postsynthetic Lanthanides Functionalization of Nanosized Metal-Organic Frameworks for Highly Sensitive Ratiometric Luminescent Thermometry

Cite this: DOI: 10.1039/x0xx00000x

Received ooth January 2012,
Accepted ooth January 2012

DOI: 10.1039/x0xx00000x

www.rsc.org/

You Zhou,[a] Bing Yan,*[a] Fang Lei [b]

A straightforward postsynthetic lanthanides functionalization strategy is developed for fabricating highly sensitive ratiometric luminescent nanothermometers based on nanosized MOFs, which highlights the opportunity of a broad range of the nanosized MOFs to construct nanothermometers.

Temperature plays crucial roles in nanotechnology and biological processes. The importance of temperature in such fields has fueled interest in the development of thermometers working at the nanosized scale and with high spatial resolution.[1] The nanothermometers based on Luminescent temperature-sensitive nanomaterials has become one of the most promising nanothermometers, owing to thier simplicity, noninvasiveness, high spatial and temporal resolution, and the ability to work even in biological fluids, strong electromagnetic fields and fast-moving objects.[2] The conventional Luminescence-based thermometry is mainly rely on the temperature-dependent fluorescence intensity of one transition, which accuracy is susceptible to error introduced by optical occlusion, concentration inhomogeneities, excitation power fluctuations, or environment-induced nonradiative relaxation. Ratiometric detection based on the intensity ratio of two independent emission of the same phosphor can circumvent these complications and give rise to more accurate self-referencing thermal sensing, thus is gaining popularity. A variety of ratiometric luminescent nanothermometers has been developed, such as organic dyes,[3] quantum dots,[4] lanthanides activated upconversion nanoparticles,[5] organic-inorganic hybrids.[6]

Recently, lanthanide luminescent metal-organic frameworks (MOFs) open a new way for ratiometric temperature detection. Cui and co-workers have pioneered a luminescent mixed lanthanide MOF approach to explore ratiometric luminescent thermometers.[7] They doped Eu^{3+} into an isostructural Tb^{3+} MOF to form the mixed lanthanide MOF $(Eu_xTb_{1-x})_2(DMBDC)_3(H_2O)_4 \cdot DMF \cdot H_2O$ in which a second emission from Eu^{3+} can be realized in addition to the original one of Tb^{3+}, while the two emissions exhibited completely opposite thermal dependence and therefore allowing for ratiometric thermometry. Since then, several ratiometric luminescent thermometers have been prepared by employing the mixed lanthanide MOF approach.[8] However, these ratiometric thermometers are not at the nanometer scale, which heavily hampers their applications in nanotechnology and biomedicine. It is thus very desirable to tailor the thermometer into nanoscale. Unfortunately, the rational design and synthesis of desired nanosized mixed lanthanide MOFs for luminescent nanothermometers remains a great challenge. Until very recently, Carlos et al. reported the first ratiometric optical MOF nanothermometer $(Tb_{0.99}Eu_{0.01}(BDC)_{1.5}(H_2O)_2)$ operative in the physiological temperature range (300-320 K), which represents an important step forward in the fabrication of nanosized MOF thermometer.[9] However, This material shows a poor sensitivity of 0.14 % $°C^{-1}$. In this contribution, we demonstrate a facile yet versatile postsynthetic approach to generate ratiometric luminescent nanothermometers with significantly enhanced sensitivities based on nanosized MOFs bearing the open bipyridine sites. Compared with the existing mixed lanthanide MOF approach for fabricating MOF nanothermometers, this strategy can circumvent the great challenge of the rational design and synthesis of nanoscale mixed lanthanide MOFs. Therefore, it represents a general yet versatile strategy and enables a broad range of the existing nanoscale MOFs for nanothermometers preparation.

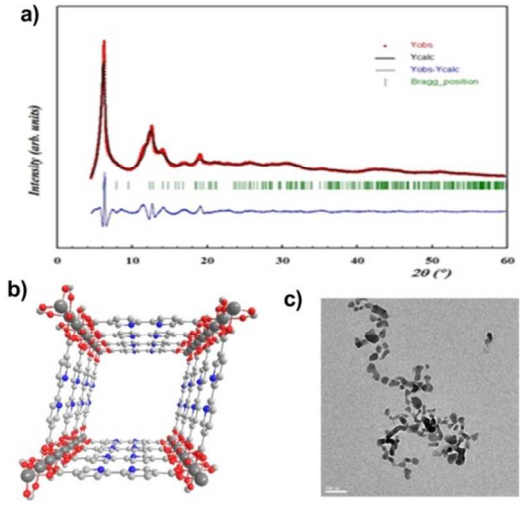

Figure 1 a) Final Rietveld plot of In(OH)(bpydc) (**1**). The observed counts and the calculated patterns are indicated by red dots and black line. The

positions of Bragg reflections are indicated by vertical bars in green and the difference between observed and calculated patterns are shown by blue line. The final fitting factors: R_p = 9.19%, R_{wp} = 13.6%, R_{exp} = 3.24%. b) Representative structure of compound **1**, with subsequent incorporation of Ln^{3+} cations into open bpy ligand site. Dark gray represent In atoms, while red, blue, light gray, and pink represent O, N, C atoms and Ln^{3+} cations. H atoms are omitted for clarity. c) TEM image of nanoparticles of **1**. The scale bar is 200 nm.

To illustrate our strategy, a MIL type MOF, In(OH)(bpydc) (bpydc = 2,2'-bipyridine-5,5'-dicarboxylic acid) was synthesized for proof of principle. The synthesis of In(OH)(bpydc) was accomplished in the direct analogy with the MOF-253.[10] Reaction of $In(NO_3)_3$ with H_2bpcdy in DMF at 150 °C for 48 h resulted a white solid. The solid was then activated by Soxhlet extraction in acetonitrile and dried under vacuum overnight to yield the fully desolvated In(OH)(bpydc) (**1**). Powder X-ray diffraction (PXRD) study (Figure 1a) showed framework **1** to be isostructural with framework Al(OH)(bpydc) (known as MOF-253). Pawley refinement of the PXRD data resulted in refined orthorhombic unit cell parameters of a = 22.44 Å, b = 6.68 Å, and c = 18.68 Å. On the basis of the refinement, it is clear that the structure of **1** is built up from chains of trans μ-OH corner-sharing InO_6-octahedra which are interconnected by $bpydc^{2-}$ ligands to form a three dimension framework with rhombic channels (Figure 1b). The crystal model of the structure is constructed by replacing Al^{3+} cations of MOF-253 with In^{3+}. It is noteworthy that the bipyridyl moieties were incorporated as free Lewis basic sites, thus allowing insertion of lanthanide cations within **1**. TEM study indicated that the as-obtained product is in the nanoscale range (40-140 nm) consisting of irregularly shaped nanoplates (Figure 1c).

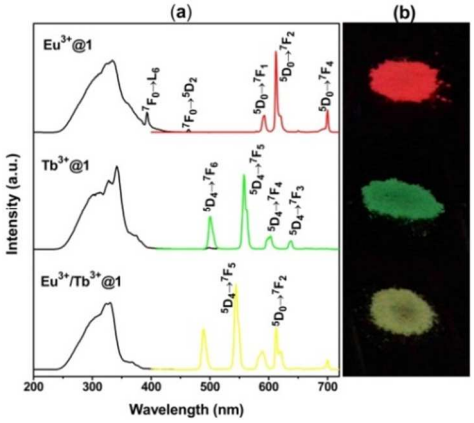

Figure 2 The excitation and emission spectra (a) and photographs illuminated with 365 nm laboratory UV light (b) of Eu^{3+}@**1**, Tb^{3+}@**1** and Eu^{3+}/Tb^{3+}@**1**.

Lanthanides post-functionalization of **1** was conducted by soaking the solid in DMF solutions of chlorine salts of Eu^{3+}, Tb^{3+}, Eu^{3+}/Tb^{3+} (0.005/0.995). The EDS and ICP-MS analysis of the resulting products indicated successful Ln^{3+} cations incorporation into framework **1** to yield Eu^{3+}@**1**, Tb^{3+}@**1** and Eu^{3+}/Tb^{3+}@**1** (Table S1, 2). The Ln^{3+} loaded samples maintain the integrity of the framework and nanoplate-morphology of **1**, as confirmed by PXRD and TEM measurements (Figure S1). Thermogravimetric analysis (Figure S2) showed these Ln^{3+}@**1** products to exhibit weight losses at 120 °C, which correspond to the adsorbed water molecules. No additional loss occurred up to 400 °C. Successful formation of Eu^{3+}@**1**, Tb^{3+}@**1** and Eu^{3+}/Tb^{3+}@**1** was also confirmed by spectroscopic studies. Upon excitation at 330 nm, Eu^{3+}@1 and Tb^{3+}@**1** exhibited characteristic sharp emissions of respective Eu^{3+} and Tb^{3+} (Figure 2a). Their multiband emissions can be realized by simultaneously encapsulation of Eu^{3+} and Tb^{3+} within **1** (Figure 2a. Under irradiation of a UV lamp, the Eu^{3+}, Tb^{3+}, Eu^{3+}/Tb^{3+} samples emitted their distinctive colors (Eu^{3+}, red; Tb^{3+}, green; Eu^{3+}/Tb^{3+}, yellow), which can be readily observed by naked eye as a qualitative indication of lanthanide sensitization (Figure 2b).[11] In addition, the long Ln^{3+} lifetimes and high quantum yields (Table 1) of these samples supports the efficient energy transfer from the sensitizer embedded in framework 1 to the Ln^{3+} cations, as well as they can utilized as excellent candidates for luminescent sensors.

Table 1 Luminescent Lifetimes (τ) and Absolute Quantum Yields (φ) of Ln^{3+}@1 (Ln^{3+} = Eu^{3+}, Tb^{3+}, Eu^{3+}/Tb^{3+})

Ln^{3+}	τ (ms)	φ (%)	λ_{ex} (nm)
Eu^{3+}	0.458 [a]	42.05	318
Tb^{3+}	0.381 [b]	36.30	314
Eu^{3+}/Tb^{3+}	0.654 [a]/0.263 [b]	41.50	312

[a] For the $^5D_0 \rightarrow {}^7F_2$ transition of Eu^{3+}, λ_{em} = 613 nm. [b] The transition $^5D_4 \rightarrow {}^7F_5$ of Tb^{3+}, λ_{em} = 545 nm.

To evaluate the potential of Ln^{3+}@**1** materials in temperature sensing, the temperature-dependent luminescence spectra and lifetimes of Ln^{3+}@**1** were performed. As presented in Figure S3 and Figure S4, the emission intensity and decay time of Tb^{3+} in Tb^{3+}@**1** decreased sharply as the temperature increased, while the luminescence and lifetime of Eu^{3+} in Eu^{3+}@**1** was not temperature sensitive and only showed very few decline. Interestingly, the temperature-dependent luminescent behavior of Eu^{3+} and Tb^{3+} in Eu^{3+}/Tb^{3+}@**1** is significantly different from those in Eu^{3+}@**1** and Tb^{3+}@**1**, respectively (Figure 3a). When the temperature increased from 10 to 60 °C, Tb^{3+} emission exhibited a much more decrease of 60%, as compared to 33% for Tb^{3+}@**1** (Figure 3b). Simultaneously, the Eu^{3+} emission in Eu^{3+}/Tb^{3+}@**1** was enhanced, which is contrary to that in Eu^{3+}@**1**.

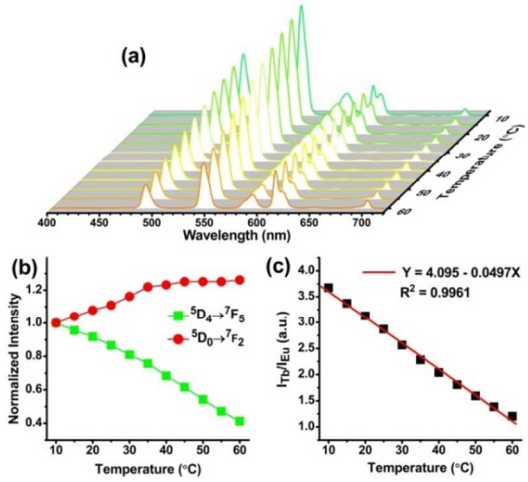

Figure 3. Eu^{3+}/Tb^{3+}@**1** nanocrystals show sensitive spectra changes in response to temperature: (a) Emission spectra (λ_{ex} = 312 nm) recorded in the temperature range of 10-60 °C; (b) temperature-dependent intensity of $^5D_4 \rightarrow {}^7F_5$ and $^5D_0 \rightarrow {}^7F_2$ transition; (c) the dependence of I_{Tb}/I_{Eu} on temperature. The red line plotted in (c) is the linear fitted curve.

The different variation of emissions of Eu^{3+} and Tb^{3+} in Eu^{3+}/Tb^{3+}@**1** with temperature enables this Ln^{3+} functionalized MOF to serve as a nanoplatform for temperature sensing. The ratiometric thermometric parameter of Eu^{3+}/Tb^{3+}@**1** can be defined as the intensity ratio of $^5D_4 \rightarrow {}^7F_5$ (Tb^{3+}, 545 nm) and $^5D_0 \rightarrow {}^7F_2$ (Eu^{3+}, 613 nm) transitions (I_{Tb}/I_{Eu}). Figure 3c plots the dependence of I_{Tb}/I_{Eu} on temperature, which reveals a good

linear relationship between I_{Tb}/I_{Eu} and temperature within the range of 10 to 60 °C. The linear relationship can be fitted as a function of equation (1) with a correlation coefficient (R^2) of 0.9961,

$$I_{Tb}/I_{Eu} = 4.95 - 0.0497T \quad (1)$$

implying that Eu^{3+}/Tb^{3+}@**1** is an excellent ratiometric nanothermometer in the range from 10 to 60 °C. The adsorption of moisture has not affected the thermometry of Eu^{3+}/Tb^{3+}@**1,** as demonstrated by the temperature-dependent emission spectra of the Eu^{3+}/Tb^{3+}@**1** product upon exposure to air for two days (Figure S5).The thermal sensitivity of Eu^{3+}/Tb^{3+}@**1** is 4.97% $°C^{-1}$, which is more than 35 times higher than that of the MOF nanothermometer $Tb_{0.99}Eu_{0.01}(BDC)_{1.5}(H_2O)_2$ (0.14% $°C^{-1}$).[9] Besides, the sensitivity of Eu^{3+}/Tb^{3+}@**1** with reported results of other types of ratiometric optical nanothermometer (in which the ratiometric value showed a linear response to temperature) is compared in Table 2. We note that the feed ratio of Tb^{3+} and Eu^{3+} has strong influence on the thermometric sensitivity of Eu^{3+}/Tb^{3+}@**1** (Figure S6 and S7). The sensitivity of Eu^{3+}/Tb^{3+}@**1** can be further enhanced to 18.8% $°C^{-1}$ by increasing the Tb^{3+}/Eu^{3+} feed ratio to 0.999/0.001. However, the precision will be reduced simultaneously because of the significant low Eu^{3+} emission will result in a low signal to noise ratio (Figure S7).

Table 2 Comparison of sensitivity of other reported ratiometric nanothermometers with ours. Materials, the temperature range of operation (ΔT), sensitivity (S).

Materials [a]	ΔT (K)	S (%K^{-1})
PFPV-RhB polymer dots [3c]	283-333	1.0
CdSe−CdS quantum dot [4a]	293-313	2.4
$NaGdF_4$:Yb^{3+}/Tm^{3+}@Tb^{3+}/Eu^{3+} NPs [5c]	125-300	1.2
CaF_2: Yb^{3+}/Tm^{3+}, Er^{3+} NPs [5a]	293-318	1.2
Eu-TTA and rhodamine 101 in PMMA core [6b]	299-313	9.3
Gd_2O_3:Yb^{3+}/Er^{3+} NPs [12]	273-473	0.2
ZnO:Er^{3+} NPs [13]	295-1000	0.6
Eu^{3+}/Tb^{3+}@**1** NPs	283-333	4.97

[a] Corresponding references.

In addition to the sensitivity, important metrics for evaluating ratiometric luminescent nanothermometers are accuracy and precision. The accuracy of Eu^{3+}/Tb^{3+}@**1** probe depends on the correlation coefficient of the calibration curve (Figure 3c). Reproducibility of the calibration curve is excellent due to the stability of Eu^{3+}/Tb^{3+}@**1** nanoparticles, as illustrated in Figure S8 and Figure S9. The precision of this thermal probe is ±0.48 °C, a value limited by the error (0.024) of I_{Tb}/I_{Eu} determined from the data in Figure 3c. The reversibility of this nanothermometer was also examined by multiple-run reversibility experiments of the I_{Tb}/I_{Eu} responses of Eu^{3+}/Tb^{3+}@**1** to temperature variation were performed (Figure S10). The data reveal that the changes of I_{Tb}/I_{Eu} are reversible in the temperature range of 10-60 °C and Eu^{3+}/Tb^{3+}@**1** nanocrytals are photostable for the duration of the 3 cycles of heating and cooling.

The different temperature dependences of Eu^{3+} and Tb^{3+} emission have also been observed in the Eu^{3+}/Tb^{3+} mixed MOFs,[7,8a,8b,9,14] and the enhancement of the Eu^{3+} emission was attributed to the thermally driven phonon-assisted Förster transfer from the Tb^{3+} to Eu^{3+} cations. To verify the applicability of this mechanism to Eu^{3+}/Tb^{3+}@**1**, the temperature-dependent emission spectra of Eu^{3+}/Tb^{3+}@**1** excited at 488 nm of the $^7F_6 \rightarrow {}^5D_4$ transition of Tb^{3+} displayed gradually enhanced Eu^{3+} emission, confirming the Tb^{3+} to Eu^{3+} energy transfer occurred and enhanced with the increase in temperature (Figure 4). Further evidence for Tb^{3+} to Eu^{3+} energy transfer was forthcoming from the $^5D_4$ and $^5D_0$ emission decay curves (Figure S11). The decay time of $^5D_4$ reduced 35% with temperature increased from 0 to 60 °C, while no apparent decrease was observed for the lifetime of $^5D_0$. It imply that the $^5D_0$ level is feeding by some source, suggesting the nonradiative energy transfer process from Tb^{3+} to Eu^{3+}. The Tb^{3+} to Eu^{3+} energy transfer efficiency ($\eta_{Tb\rightarrow Eu}$) can be determined by equation (2)[15]

$$(\eta_{Tb\rightarrow Eu}) = 1 - \tau/\tau_0 \quad (2)$$

Here, τ and τ_0 are $^5D_4$ donor lifetimes in the presence and absence of the Eu^{3+} acceptors, respectively. The value of $\eta_{Tb\rightarrow Eu}$ is estimated to be 31% at room temperature (25 °C), which is reasonably close to the value (23.1%) reported by Carlos et al.[10] As for the temperature dependence of Tb^{3+} emission in Eu^{3+}/Tb^{3+}@**1** (decreases sharply as temperature rise), it can be ascribed to the thermal activation of nonradiative relaxation including the energy transfer from Tb^{3+} to Eu^{3+} (mentioned above) and energy back transfer (BEnT) from the emitting level of the Tb^{3+} to the excited triplet state of the H_2bpydc ligand. The BEnT process is verified by the comparison temperature-dependent emission spectra of $TbCl_3$ (Figure S12) and Tb^{3+}@**1** (Figure S3).

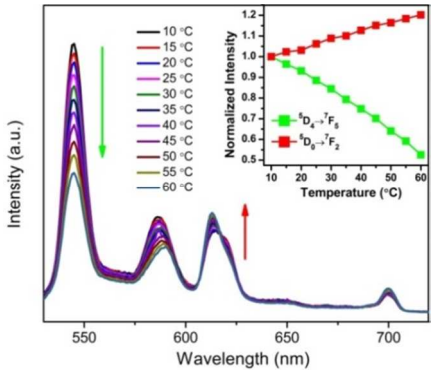

Figure 4. Emission spectra (λ_{ex} = 487 nm) of Eu^{3+}/Tb^{3+}@**1** recorded between 10 and 60 °C. The inset is the temperature-dependent normalized intensity of Eu^{3+} ($^5D_0 \rightarrow {}^7F_2$) and Tb^{3+} ($^5D_4 \rightarrow {}^7F_5$).

Another indication provided from Figure 4 is that Eu^{3+}/Tb^{3+}@**1** nanoparticles can also be developed as ratiometric optical thermometers when the excitation wavelength is fixed at 487 nm. The temperature (10-60 °C) can be related to I_{Tb}/I_{Eu} by a linear calibration curve with a slope of -3.69% (Figure S13). This thermometric sensitivity is lower than that of Eu^{3+}/Tb^{3+}@**1** when employing 312 nm excitation (4.97% $°C^{-1}$). Nevertheless, 487 nm excitation is much less cytotoxic than 320 nm, thus is preferred in biotechnology.

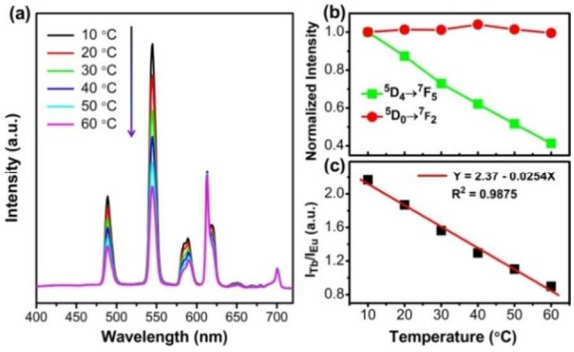

Figure 5 (a) Emission spectra of Eu^{3+}/Tb^{3+}@**2** recorded btween 10 and 60 °C, (b) temperature-dependent normalized intensity of Eu^{3+} ($^5D_0 \rightarrow {}^7F_2$) and Tb^{3+} ($^5D_4 \rightarrow {}^7F_5$) for Eu^{3+}/Tb^{3+}@**2** and (c) the dependence of I_{Tb}/I_{Eu} on temperature for Eu^{3+}/Tb^{3+}@**2**. The red line plotted in (c) is the linear fitted curve.

The applicability of this Ln^{3+} functionalized MOF strategy to two isostructural nanosized MOFs of 1, MOF-253 (**2**) and Ga(OH)(bpydc) (**3**, known as COCMOC-4), were also demonstrated. Immersing the nanocrytsals of **2** and **3** in DMF solutions of chlorine salts of Eu^{3+} and Tb^{3+} afforded Eu^{3+}/Tb^{3+}@**2** and Eu^{3+}/Tb^{3+}@**3**. Their identities and morphologies were determined by PXRD and TEM studies (Figure S14, 15).[11,16] Figure 5 and Figure S16 presents the respective temperature dependence of emission spectra of Eu^{3+}/Tb^{3+}@**2** and Eu^{3+}/Tb^{3+}@**3**, in which similar luminescent behavior on temperature to that of Eu^{3+}/Tb^{3+}@**1** are observed. With temperature increases, the Tb^{3+} emission of these products decreases rapidly, while the Eu^{3+} emission is slightly enhanced. The temperature can be linearly related to the intensity ratio of $^5D_4 \rightarrow {}^7F_5$ (Tb^{3+}, 545 nm) and $^5D_0 \rightarrow {}^7F_2$ (Eu^{3+}, 613 nm) transitions of both Eu^{3+}/Tb^{3+}@**2** and Eu^{3+}/Tb^{3+}@**3**, revealing they can serve as ratiometric nanothermometers in temperature range from 10 to 60 °C. However, they afford lower sensitivities (2.54 % $°C^{-1}$ for Eu^{3+}/Tb^{3+}@**2** and 1.97% $°C^{-1}$ for Eu^{3+}/Tb^{3+}@**3**) in comparison with Eu^{3+}/Tb^{3+}@**1**.

In summary, we have described an Ln^{3+} post-functionalized MOF approach for the generation of ratiometric luminescent nanothermometers, as exemplified by insertion of Ln^{3+} cations within **1** and its two isostructural MOFs (**2** and **3**) for nanothermometers. Compared with the existing mixed lanthanide MOF approach, this strategy can circumvent the great challenge of the rational design and synthesis of nanoscale mixed lanthanide MOFs. Therefore, it represents a facile yet versatile pathway and provides new opportunities for the existing MOFs to construct nanotermometers. Furthermore, the optical nanothermometers prepared via this Ln^{3+} functionalized approach show significantly enhanced sensitivities in comparison with $Tb_{0.99}Eu_{0.01}(BDC)_{1.5}(H_2O)_2$. We expect these nanosized thermometers with high sensitivity and self-referencing output will have potential use in nanotechnology and biomedicine.

Acknowledgements

This work was supported by the National Natural Science Foundation of China (91122003) and Developing Science Funds of Tongji University. We thank Dr. H. H. Chen for technical support.

Notes and references

[a] Department of Chemistry, Tongji University, Shanghai, 200092, China. E-mail: byan@tongji.edu.cn; Tel: +86-21-65984663
[b] School of Materials Science and Engineering, Shanghai University, Shanghai 200072, China

† Electronic Supplementary Information (ESI) available: [details of any supplementary information available should be included here]. See DOI: 10.1039/b000000x/

1 (a) Z. G. Yang, J. F. Cao, Y. X. He, J. H. Yang, T. Kim, X. J. Peng and J. S. Kim, *Chem. Soc. Rev.*, 2014, **43**, 4563; (b) D. Jaque, B. del Rosal, E. M. Rodriguez, L. M. Maestro, P. Haro-Gonzalez and J. G. Sole, *Nanomedicine*, 2014, **9**, 1047; (c) C. D. S. Brites, P. P. Lima, N. J. O. Silva, A. Millan, V. S. Amaral, F. Palacio and L. D. Carlos, *Nanoscale*, 2012, 4, 4799; (d) Y. H. Gao and Y. Bando, *Nature*, 2002, **415**, 599; (e) C. Gota, K. Okabe, T. Funatsu, Y. Harada and S. Uchiyama, *J. Am. Chem. Soc.*, 2009, **131**, 2766.
2 (a) E. J. McLaurin, L. R. Bradshaw and D. R. Gamelin, *Chem. Mater.*, 2013, 25, 1283; (b) Z. X. Gan, X. L. Wu, J. L.Zhang, X. B. Zhu and P. K. Chu, *Biomacromolecules*, 2013, **14**, 2112; (c) X. D. Wang, O. S. Wolfbeis and R. J. Meier, *Chem. Soc. Rev.*, 2013, 42, 7834; (d) A. Balamurugan, M. L. P. Reddy and M. Jayakannan, *J. Mater. Chem. A*, 2013, **1**, 2256.
3 (a) K. Okabe, N. Inada, C. Gota, Y. Harada, T. Funatsu and S. Uchiyama, *Nat. Commun.*, 2012, **3**, 705; (b) C. Y. Chen and C. T. Chen, *Chem. Commun.*, 2011, **47**, 994; (c) F. M. Ye, C. F. Wu, Y. H. Jin, Y. H. Chan, X. J. Zhang and D. T. Chiu, *J. Am. Chem. Soc.*, 2011, **133**, 8146.
4 (a) A. E. Albers, E. M. Chan, P. M. McBride, C. M. Ajo-Franklin, B. E. Cohen and B. A. Helms, *J. Am. Chem. Soc.*, **2012**, 134, 9565; (b) E. J. McLaurin, V. A. Vlaskin and D. R. Gamelin, *J. Am. Chem. Soc.*, **2011**, 133, 14978; (c) S. L. Shinde and K. K. Nanda, *Angew. Chem., Int. Edit.*, **2013**, 52, 11325.
5 (a) N. N. Dong, M. Pedroni, F. Piccinelli, G. Conti, A. Sbarbati, J. E. Ramirez-Hernandez, L. M. Maestro, M. C. Iglesias-de la Cruz, F. Sanz-Rodriguez, A. Juarranz, F. Chen, F. Vetrone, J. A. Capobianco, J. G. Sole, M. Bettinelli, D. Jaque and A. Speghini, *ACS Nano*, 2011, **5**, 8665; (b) M. L. Debasu, D. Ananias, I. Pastoriza-Santos, L. M. Liz-Marzan, J. Rocha and L. D. Carlos, *Adv. Mater.*, 2013, **25**, 4868; (c) S. H. Zheng, W. B. Chen, D. Z. Tan, J. J. Zhou, Q. B. Guo, W. Jiang, C. Xu, X. F. Liu and J. R. Qiu, *Nanoscale*, 2014, **6**, 5675.
6 (a) C. D. S. Brites, P. P. Lima, N. J. O. Silva, A. Millan, V. S. Amaral, F. Palacio and L. D. Carlos, *Adv. Mater.*, 2010, **22**, 4499; (b) Y. Takei, S. Arai, A. Murata, M. Takabayashi, K. Oyama, S. Ishiwata, S. Takeoka and M. Suzuki, *ACS Nano*, 2014, **8**, 198.
7. Y. J. Cui, H. Xu, Y. F. Yue, Z. Y. Guo, J. C. Yu, Z. X. Chen, J. K. Gao, Y. Yang, G. D. Qian and B. L. Chen, *J. Am. Chem. Soc.*, 2012, **134**, 3979.
8 (a) X. T. Rao, T. Song, J. K. Gao, Y. J. Cui, Y. Yang, C. D. Wu, B. L. Chen and G. D. Qian, *J. Am. Chem. Soc.*, 2013, **135**, 15559; (b) Y. J. Cui, W. F. Zou, R. J. Song, J. C. Yu, W. Q. Zhang, Y. Yang and G. D. Qian, *Chem. Commun.*, 2014, **50**, 719; (c) R. F. D'Vries, S. Alvarez-Garcia, N. Snejko, L. E. Bausa, E. Gutierrez-Puebla, A. de Andres and M. A. Monge, *J. Mater. Chem. C*, 2013, **1**, 6316.
9 A. Cadiau, C. D. S. Brites, P. M. F. J. Costa, R. A. S. Ferreira, J. Rocha and L. D. Carlos, *ACS Nano*, 2013, **7**, 7213.
10 E. D. Bloch, D. Britt, C. Lee, C. J. Doonan, F. J. Uribe-Romo, H. Furukawa, J. R. Long and O. M. Yaghi, *J. Am. Chem. Soc.*, 2010, **132**, 14382.
11 (a) Y. Zhou and B. Yan, *Inorg. Chem.*, 2014, **53**, 3456; (b) J. Y. An, C. M. Shade, D. A. Chengelis-Czegan, S. Petoud and N. L. Rosi, *J. Am. Chem. Soc.*, 2011, **133**, 1220.
12 S. K. Singh, K. Kumar and S. B. Rai, *Sensor Actuat a-Phys*, 2009, **149**, 16.
13 X. Wang, X. G. Kong, Y. Yu, Y. J. Sun and H. Zhang, *J. Phys. Chem. C*, 2007, **111**, 15119.
14 K. Miyata, Y. Konno, T. Nakanishi, A. Kobayashi, M. Kato, K. Fushimi and Y. Hasegawa, *Angew. Chem., Int, Edi.*, 2013, **52**, 6413.
15 (a) M. O. Rodrigues, J. D. L. Dutra, L. A. O. Nunes, G. F. de Sa, W. M. de Azevedo, P. Silva, F. A. A. Paz, R. O. Freire and S. A. Junior, *J. Phys. Chem. C*, 2012, **116**, 19951; (b) C. Piguet, J. C. G. Buzli, G. Bernardinelli, G. Hopfgartner, A. F. Williams, *J. Am. Chem. Soc.* 1993, **115**, 8197.
16 Y. Y. Liu, R. Decadt, T. Bogaerts, K. Hemelsoet, A. M. Kaczmarek, D. Poelman, M. Waroquier, V. Van Speybroeck, R. Van Deun and P. Van Der Voort, *J. Phys. Chem. C*, 2013, **117**, 11302.

